MANCHESTER 1824
The University of Manchester

The University of Manchester Research

Model Predictive Control for optimizing the flexibility of sustainable energy assets: An experimental case study

DOI:
10.1016/j.ijepes.2021.106822

Document Version
Accepted author manuscript

Link to publication record in Manchester Research Explorer

Citation for published version (APA):
Bolzoni, A., Parisio, A., Todd, R., & Forsyth, A. (2021). Model Predictive Control for optimizing the flexibility of sustainable energy assets: An experimental case study. *International Journal of Electrical Power & Energy Systems*, *129*, 106822. https://doi.org/10.1016/j.ijepes.2021.106822

Published in:
International Journal of Electrical Power & Energy Systems

Citing this paper
Please note that where the full-text provided on Manchester Research Explorer is the Author Accepted Manuscript or Proof version this may differ from the final Published version. If citing, it is advised that you check and use the publisher's definitive version.

General rights
Copyright and moral rights for the publications made accessible in the Research Explorer are retained by the authors and/or other copyright owners and it is a condition of accessing publications that users recognise and abide by the legal requirements associated with these rights.

Takedown policy
If you believe that this document breaches copyright please refer to the University of Manchester's Takedown Procedures [http://man.ac.uk/04Y6Bo] or contact uml.scholarlycommunications@manchester.ac.uk providing relevant details, so we can investigate your claim.

OPEN ACCESS

Download date:09. Jun. 2022

Model Predictive Control for optimizing the flexibility of sustainable energy assets: an experimental case study.

Alberto Bolzoni, Alessandra Parisio, Rebecca Todd, Andrew Forsyth.

Authors are with the Department of Electrical and Electronic Engineering, at The University of Manchester, Manchester, UK (alberto.bolzoni@manchester.ac.uk, alessandra.parisio@manchester.ac.uk, Andrew.Forsyth@manchester.ac.uk).

This work was supported in part by the project *Q-PLUS Intelligent Building energy management system utilizing energy storag*e, Innovate UK Technology Strategy Board, n.133463, and also by the project *MANIFEST* of the UK Engineering and Physical Sciences Research Council EPSRC - EP/N032888/1.

ABSTRACT:
A detailed system-level Model Predictive Control (MPC) framework is developed for use with sustainable technology systems which have either electrical or thermal load flexibility. Differently from the majority of relevant works in the literature, the proposed MPC framework includes non-ideal conversion efficiencies, flexibility in electrical/thermal loads and a detailed battery degradation model. A hybrid PV estimator based on clear-sky models and actual measurements is exploited for the photovoltaic production prediction within the MPC optimization problem. The formulated MPC problem is multi-objective, which aims to maximize the profit from energy arbitrage and minimise carbon emissions via a sustainable technology weighting factor (λ_{CI}). A key novelty of the proposed approach is associated with the real-time experimental testing of the MPC framework using a microgrid consisting of an actual energy storage asset, a PV system and two buildings with electrically powered thermal loads. The experimental setup comprises a Hardware-in-the-loop (HIL) system together with a physical 240 kW 180 kWh battery energy storage system and a Real Time Digital Simulator (RTDS). Three scenarios with differing levels of flexibility in the electrical and thermal loads are considered, so as to derive consistent comparisons. When flexibility in both the electrical and thermal loads is utilised, a CO_2 reduction of up to 75 kg/day (λ_{CI}=0.01) and an energy saving of up to 50 £/day (λ_{CI} =0) is observed, yielding a reduction of around 10% in carbon emissions or energy consumption with respect to the base case.

KEYWORDS:
Building energy management; Energy storage; Model Predictive Control; Microgrids; Sustainable energy assets.

NOMENCLATURE

Indexes and MPC parameters

H, h	total prediction horizon and its index
$\Delta t, k$	discrete-time step and its index
$i = 1 \dots N^{st}$	index for storage units
$b = \{A, B..\}$	index for buildings
$n = 1 \dots N_b^{tz}$	index for thermal zones in each building
T_s	RTDS real-time Hardware-in-the-Loop step

Storage parameters and variables

P_i^{st}	actual storage production
$\overline{P_i^{st}}$, $\underline{P_i^{st}}$	max and min storage power levels
η_i^{ch}, η_i^{dis}	charging, discharging efficiencies
SoC_i, E_i	storage state of charge, nominal energy
$\overline{SoC_i}$, $\underline{SoC_i}$	max and min state of change levels
z_i^{st}, δ_i^{st}	additional storage decision variables

Building related parameters and variables

P_b^{bu}	total building consumption
P_b^{el}	unregulated building electrical loads
$\dot{Q}_{n\,b}$	heat injection in each thermal zone
$COP_{n\,b}$	thermal-zone Coefficient of Performance
$\vartheta_{n\,b}$	thermal zone temperature
$\overline{\vartheta_{n\,b}}, \underline{\vartheta_{n\,b}}$	thermal zone temperature max / min limits
ϑ_a	ambient temperature
$C_{n\,b}^{th}, G_{n\,b}^{th}$	thermal zone capacitance, conductance
$O_{n\,b}$	thermal zone occupancy
$p_{n\,b}$	occupancy to temperature impact coefficient
$s_{n\,b}$	direct solar irradiance to temperature coefficient

PV and irradiance model parameters

Ir^{meas}/ Ir^{h}	measured / estimated solar irradiance
Ir^{stc}	standard test conditions solar irradiance
Ir^{CS}	maximum (clear-sky) solar irradiance
P^{PV}, $P^{PV\,h}$	actual / estimated photovoltaic production
$\overline{P^{PV}}$	nominal photovoltaic size
ϕ, ξ	site latitude and zenith angle
γ, χ	clear-sky parameters
d, sh	day number and solar hour in clear-sky model

External grid balance

P^g	power injected into the grid
$\overline{P^g}$, $\underline{P^g}$	max and min storage power levels
z^g, δ^g	auxiliary variables for grid-power sign tracking

Cost function related parameters

C_A	energy-arbitrage cost
C_{CI}	carbon-intensity cost
C_1, C_2	battery-ageing cost
$c(k)$	carbon intensity at time k
λ_b, λ_s	energy buy / sell prices
λ_{CI}	user-defined sustainability factor (£/gCO_2)
$\lambda_{1i}, \lambda_{2i}$	battery-ageing coefficients

1. Introduction

1.1. The context

Greenhouse gas emissions are undoubtedly one of the major causes of global climate change. A radical reduction in carbon footprint can be achieved through the adoption of integrated energy policies, which include the containment of consumption, the de-carbonization of the energy supply and the lowering of atmospheric emissions [1]. Furthermore, the coordinated management of energy vectors is also beneficial for the end-users in terms of reduced operating costs and security of the supply. In this perspective, National Grid (UK TSO) identifies the electrification of domestic and commercial buildings heating systems as a near-term alternative to the well-established gas-combustion boilers [2]: the coordinated control of heating and electrical units then acquires an unprecedented importance and represents a clear opportunity to reduce the environmental/economic impact of energy consumption.

In this paper, a Model Predictive Control (MPC) approach is adopted for this purpose: compared to heuristic or empirical techniques, MPC guarantees an optimized trajectory of the system, a robust behaviour against unmodelled dynamics and the fulfilment of the operating constraints associated with the physical assets [3].

1.2. Literature and state-of-the art analysis

Several works in the literature show how MPC has been successfully applied to the field of electrical grid operation management. The MPC technique is exploited in [4] to minimize the voltage and frequency deviation experienced in an island-operated microgrid, with storage devices and renewable generators; a similar approach is proposed in [5], to balance the injections from a fleet of battery storage systems. In [6] several flexibility assets (battery storage, renewable generators, diesel gen-sets) are coordinated in order to maximize the system profitability during market operations, even though important aspects like battery degradation models are not included. Most of these publications assumes off-line idealized conditions, rather than a real-time implementation of the proposed techniques [7]-[8]. Furthermore, they do not explicitly include the interaction between the electrical assets and other relevant dynamics associated to the local loads (e.g. the thermal vectors involved in the buildings temperature control).

Some early works on this topic analyse the regulation of building thermal dynamics through MPC approaches for minimizing the energy usage under natural weather variability while guaranteeing occupants' comfort [9]-[10]. Nevertheless, the focus of these studies is predominantly focused on single buildings rather than on the whole-system level, and the optimization objective is exclusively related to economic factors with no consideration of environmental aspects. A few recent studies have started exploring the benefits brought by the optimal management of the flexibility afforded by buildings combined with energy storage systems [11]-[14], which can also incorporate energy arbitrage functions: while the publications so far have demonstrated promising results from MPC frameworks, they often lack consideration of essential aspects such as flexible loads, CO_2 emissions or battery degradation, and generally no real-time algorithm experimental implementation is performed. Furthermore, the energy storage models utilised in some of the proposed frameworks are excessively simplified, do not clearly rule out the possibility of having simultaneous charging and discharging conditions and rarely include non-ideal conversion efficiencies. Other studies [15] include detailed models of the building thermal management, but exploit a simplified representation for renewables, do not analyse the environmental sustainability aspects and assess the proposed approach through simulation instead of experiments.

1.3. Main contributions

Differently from the available literature on the topic, this paper aims at deriving a holistic MPC approach for a grid-connected microgrid composed of a wide range of flexibility assets (e.g., battery storage, renewable generators and building thermal control), including a detailed representation of the dynamical electrical/thermal coupling between the comprised energy sources. The key contribution of the paper includes both the mathematical modelling of the system and its operation optimization, and its real-time experimental assessment.

As to the mathematical modelling of the system and its operation optimization, the developed control framework consists of a detailed system-level MPC optimization model, which combines electrical/thermal coupling dynamics, heat control, electrochemical storage devices and renewable generation at a unified mathematical model. This system-level model includes also non-ideal conversion efficiencies, flexible electrical/thermal loads and detailed battery degradation models are also included. Furthermore, both the maximization of the profit from energy arbitrage and the reduction of carbon emissions are integrated into the proposed multi-objective MPC optimization problem, which is able to achieve an optimal trade-off between the economic and environmental needs through the sustainable technology weighting factor ($\boldsymbol{\lambda_{CI}}$). These aspects have never been analysed together, to the best of the author's knowledge.

In addition, differently from the majority of the relevant studies in the literature, the prosed MPC-based optimization is integrated into a flexible hybrid experimental set-up (hardware + HIL), which enables a consistent performance assessment under real-time high-fidelity conditions and allows to stress-test the algorithm capabilities in a scenario close to the real network operations. A hardware grid-scale 240 kVA 180 kWh battery storage system is integrated in the set-up and experimental profiles of the buildings consumption and renewable generation are exploited. Similarly, the evaluation of the environmental impact of the developed control strategy obtained through the proposed multi-objective optimization includes the real carbon intensity profiles of the UK energy scenario: this allows to derive an extensive and consistent validation of the algorithm performance.

1.4. Paper outlines

The paper is organized as follows: in Section 2 the dynamic models of the system are introduced, while Section 3 outlines the optimization algorithm. The real-time experimental set-up is described in Section 4, together with a detailed analysis of the technical and computational aspects associated with the real-time resolution of the optimization problem. The experimental

results plus discussion are reported in Section 5, before the conclusion of the work.

1. System modelling

1.1. Storage system model

Each storage unit $i = 1 \dots N^{st}$ is modelled as a discrete-time difference equation:

$$SoC_i(k+1) = SoC_i(k) + \eta_i \frac{P_i^{st}(k)}{E_i} \Delta t \qquad (1)$$

where η_i is the conversion efficiency given by (2). The battery State of Charge SoC range in (1) is $SoC_i \in [\underline{SoC_i};\ \overline{SoC_i}]$, while $P_i^{st}(k)$ is the battery power in [kW] (positive when charging), and is physically bounded by the rating of the converter $P_i^{st}(k) \in \left[\underline{P_i^{st}};\ \overline{P_i^{st}}\right]$; Δt is the sample period and E_i [kWh] is the nominal energy content of the battery asset.

$$\eta_i = \begin{cases} \eta_i^{ch} & if\ P_i^{st}(k) \geq 0 \\ \dfrac{1}{\eta_i^{dis}} & \text{otherwise} \end{cases} \qquad (2)$$

Due to the different charging and discharging efficiencies in (2), binary variables need to be associated with the storage model, which will lead to a Mixed-Integer Linear Problem (MILP) formulation of the optimization problem in Section 3. MILPs can be solved by computationally-efficient numerical techniques (e.g., branch-and-bound).

As used in the storage model proposed in [6], and based on the formalisation described in [16], an integer binary value $\delta_i^{st}(k) \in \{0,1\}$, $\delta_i^{st}(k) = 1$ charging, $\delta_i^{st}(k) = 0$ discharging, is introduced to model the battery charging/discharging mode, i.e., $P_i^{st}(k) \geq 0 \leftrightarrow \delta_i^{st}(k) = 1$. Equation (3) describes the mixed-integer linear inequalities related to $\overline{P_i^{st}}$ and $\underline{P_i^{st}}$. The very small tolerance ε is introduced into the $\overline{P_i^{st}}$ equation in (3) as MILP algorithms require non-strict inequalities; the $\underline{P_i^{st}}$ equation naturally satisfies the inequality requirement.

$$\begin{cases} P_i^{st}(k) - \left(\overline{P_i^{st}} + \varepsilon\right)\delta_i^{st}(k) + \varepsilon \leq 0 \\ -P_i^{st}(k) + \underline{P_i^{st}}\left(1 - \delta_i^{st}(k)\right) \leq 0 \end{cases} \qquad (3)$$

The auxiliary real variable $z_i^{st}(k) = \delta_i^{st}(k) P_i^{st}(k)$ is introduced to express (1) and (2) combined as a linear equation subject to the constraint $SoC_i(k) \in [\underline{SoC_i};\ \overline{SoC_i}]$:

$$SoC_i(k+1) = SoC_i(k) + \left(\eta_i^{ch} - \frac{1}{\eta_i^{dis}}\right)\frac{\Delta t}{E_i} z_i^{st}(k) + \\ + \frac{1}{\eta_i^{dis}}\frac{\Delta t}{E_i} P_i^{st}(k) \qquad (4)$$

In order to yield a MILP formulation, the non-linearity in the definition of the auxiliary variable $z_i^{st}(k)$ has to be expressed as a system of linear mixed-integer inequalities [6], [16]:

$$\begin{cases} z_i^{st}(k) - \overline{P_i^{st}}\delta_i^{st}(k) \leq 0 \\ -z_i^{st}(k) + \underline{P_i^{st}}\delta_i^{st}(k) \leq 0 \\ z_i^{st}(k) - P_i^{st}(k) + \underline{P_i^{st}}\left(1 - \delta_i^{st}(k)\right) \leq 0 \\ -z_i^{st}(k) + P_i^{st}(k) - \overline{P_i^{st}}\left(1 - \delta_i^{st}(k)\right) \leq 0 \end{cases} \qquad (5)$$

Thus the dynamics of each storage asset can be expressed in compact form by the linear equality (4), and the mixed-integer linear vector inequality (6)

$$\boldsymbol{M_P} P_i^{st} + \boldsymbol{M_\delta}\, \delta_i^{st} + \boldsymbol{M_z}\, z_i^{st} + \boldsymbol{M_{SoC}} SoC_i \leq \boldsymbol{M_t} \qquad (6)$$

$$\boldsymbol{M_P} = [1 \quad -1 \quad 0 \quad 0 \quad -1 \quad 1 \quad 0 \quad 0]^T$$

$$\boldsymbol{M_\delta} = \left[-\overline{P_i^{st}} - \varepsilon \quad -\underline{P_i^{st}} \quad \overline{P_i^{st}} \quad \underline{P_i^{st}} \quad -\underline{P_i^{st}} \quad \overline{P_i^{st}} \quad 0 \quad 0\right]^T$$

$$\boldsymbol{M_z} = [0 \quad 0 \quad 1 \quad -1 \quad 1 \quad -1 \quad 0 \quad 0]^T$$

$$\boldsymbol{M_{SoC}} = [0 \quad 0 \quad 0 \quad 0 \quad 0 \quad 0 \quad 1 \quad -1]^T$$

$$\boldsymbol{M_t} = \left[-\varepsilon \quad -\underline{P_i^{st}} \quad 0 \quad 0 \quad -\underline{P_i^{st}} \quad \overline{P_i^{st}} \quad \overline{SoC_i} \quad \underline{SoC_i}\right]^T.$$

1.2. Building model

The electrical consumption P_b^{bu} of each building (identified by the index $b = \{A, B, C \dots\}$) is modelled in (7) as the sum of two independent contributions: *i*) P_b^{el}, which is associated with the uncontrollable electrical loads; *ii*)the summation term in (7), which is related to the temperature control and takes into account the electrical consumption of the heat pumps within each thermal zone, the latter identified by the index $n = 1 \dots N_b^{tz}$:

$$P_b^{bu}(k) = P_b^{el}(k) + \textstyle\sum_{n=1}^{N_b^{tz}} \dot{Q}_{n\,b}(k) \,/\, COP_{n\,b}, \qquad (7)$$

where $\dot{Q}_{n\,b}(k)$ is the heat injection in each thermal zone, and $COP_{n\,b}$ is the Coefficient of Performance of the thermal unit.

Fig. 1 shows the measured consumption profiles P_b^{el} of two buildings in Manchester (a university building (a) and a commercial building (b)) over an observation period of one year. Both P_b^{el} profiles show a predominant weekly periodicity in the absorbed electrical power, thus the seven-days-ahead hourly consumption can be reasonably utilized as a forecast of P_b^{el} within the MPC framework.

The thermal dynamics are included following the procedure in [17]. The temperature evolution is:

$$\vartheta_{n\,b}(k+1) = \vartheta_{n\,b}(k) + C_{n\,b}^{th\ -1}\left[\left(\vartheta_a(k) - \vartheta_{n\,b}(k)\right)G_{n\,b}^{th} + \right. \\ \left. + \dot{Q}_{n\,b}(k) + s_{n\,b}\, Ir^{meas}(k) + p_{n\,b} O_{n\,b}(k)\right]\Delta t\,, \qquad (8)$$

where $\vartheta_{n\,b}(k)$ is the thermal zone temperature, $C_{n\,b}^{th}$ corresponds to the thermal capacitance in [J/K], $G_{n\,b}^{th}$ is the thermal-zone to ambient thermal conductance [W/K], $\dot{Q}_{n\,b}$ is the thermal flux controlled by the temperature management system, and $Ir^{meas}(k)$ and $O_{n\,b}(k)$ are the solar irradiance (described in Section 2.3) and people occupancy respectively.

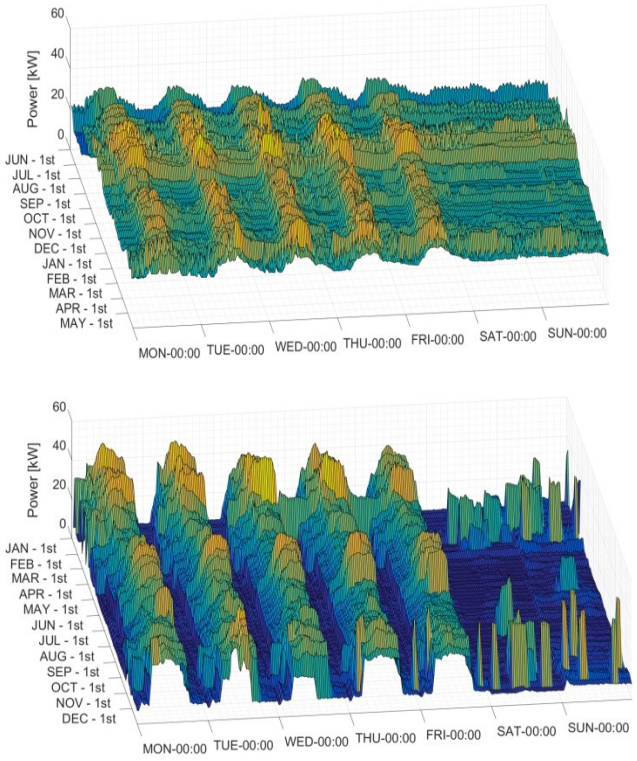

Fig. 1: Experimental consumption profiles of (a) university building and (b) a commercial site (thermal management units excluded).

The coefficients $s_{n\,b}$ and $p_{n\,b}$ determine the dependence of each thermal zone on people occupancy and solar radiation. The parameters $G_{n\,b}^{th}$, $C_{n\,b}^{th}$, $s_{n\,b}$, $p_{n\,b}$, with $b = \{A, B \dots\}$ and $n = \{1 \dots N_b^{tz}\}$, in (8) are estimated using datasets obtained from Energy+ models of the considered buildings; the Energy+ models have been validated against actual measurements [18]. A least-square parametric identification approach [19] is adopted to estimate the optimal values of the unknown parameters $(G_{n\,b}^{th}, C_{n\,b}^{th}, s_{n\,b}, p_{n\,b})$, with the input dataset comprising the measured temperature $\vartheta_{n\,b}$ and the known inputs $\dot{Q}_{n\,b}, \vartheta_a, Ir^{meas}, O_{n\,b}$.

As the thermal dynamics of the system involve a significant amount of absorbed energy from the grid, they significantly affect the economical / environmental costs associated with the system. Smart management of their energy absorption profiles can deliver a substantial improvement in the microgrid management, as demonstrated in Section 5.

1.3. PV generation

The renewable source considered in this case study is a photovoltaic (PV) system, which is modelled as a time-varying power source with an instantaneous solar irradiance of $Ir(k)$. The inherent coupling of the PV generation with the buildings thermal evolution provides the best scenario to test the capabilities of the proposed integrated approach. The actual instantaneous power produced by the PV system is obtained from the measured Ir^{meas} and standard-test Ir^{stc} irradiance (Ir^{stc}=1000 W/m^2) as:

$$P^{PV}(k) = -Ir^{meas}(k) \cdot \overline{P^{PV}}/Ir^{stc} \tag{9}$$

The negative sign in (9) is introduced to keep a consistent convention with the one adopted for the storage unit (negative power when physically injected).

To exploit the optimal control capabilities in optimizing the system dynamics with respect to upcoming disturbances, a real-time estimator of the future irradiance profile is needed by the MPC. Offline Artificial Neural Networks and statistical techniques have both been proposed as PV forecasters in recent years; however, the computational effort associated with the algorithm convergence and the huge amount of historical data required for the training make them unsuitable for online applications [20]-[22]. Another option, with reduced computational needs, is an algebraic estimator based on the clear-sky algorithm for real-time short-term prediction. Following the Robledo-Soler approach [23], the algorithm accepts as input the latitude ϕ of the considered site and predicts the maximum global horizontal irradiance Ir^{CS} (11) as a function of the solar zenith angle ξ defined in (10):

$$\xi = \text{acos}(\cos(\phi)\cos(\gamma)\cos(\chi) + \sin(\phi)\sin(\gamma)) \tag{10}$$

$$Ir^{CS}(k) = \max\left(1159.24[cos(\xi)]^{1.179} e^{-0.019\,(90-\xi)}, 0\right) \tag{11}$$

where γ and χ in (10) are function of the day within the year d and the solar hour sh, according to:

$$\gamma = 23.26 \sin\left(360^o \frac{d-81}{365}\right) \quad \chi = (sh - 12) \cdot 15^o \tag{12}$$

Equation (13) extends the clear-sky approach to take into account for the actual weather conditions through an online adaptive factor that rescales the forecasted theoretical production Ir^{CS}, function of the last measurements available. Thus the h-steps ahead estimator of the solar irradiance $Ir^h(k)$ and PV production $P^{PV\,h}(k)$ for $h \in [1, H]$ are:

$$Ir^h(k) = \frac{Ir^{meas}(k)}{Ir^{CS}(k)} \cdot Ir^{CS}(k+h), \tag{13}$$

$$P^{PV\,h}(k) = -Ir^h(k) \cdot \overline{P^{PV}}/Ir^{stc} \tag{14}$$

Fig. 2 shows the performance of the clear-sky estimator (11), the proposed estimator (13) as a function of the prediction index h, and the actual measured profile taken from a real PV both sunny (left) and partially-cloudy (right) days.

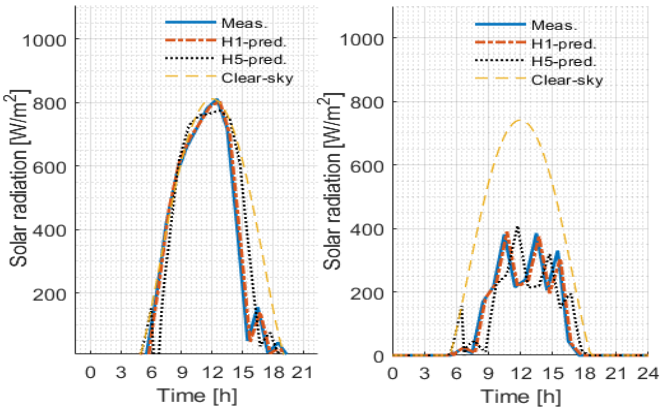

Fig. 2: Actual solar irradiance injection, h1-prediction ($h = 1$) and h5-prediction ($h = 5$) for a sunny (on the left) and cloudy day (on the right).

The analysis reveals that for clear days (Fig. 2-left) the proposed predictor converges to the actual measured state, both for the short-term ($h = 1$, which corresponds to a forecast of Δt=15 min) and mid-term prediction ($h = 5$, corresponding to an horizon of $5\Delta t$); on partially-cloudy days (Fig. 2, right), the quality of the forecaster slightly degrades for mid-term predictions, while it remains reliable for the short-term $h = 1$ prediction. Comparing the hybrid estimator (13) with the clear-sky estimator (11) for the cloudy day (e.g. the one in Fig. 2-left, for $h = 5$), leads to a RMS error reduction from 232.7 W/m^2 (clear-sky) to 68.7 W/m^2 (hybrid) with respect to the actual measurements.

Furthermore, the intrinsic feedback mechanism introduced by the MPC scheme during real-time operation is able to partially compensate for the uncertainty associated with the hybrid estimator.

1.4. Grid balance

The physical connection of the different assets is modelled as a power balance equality constraint, where P^g is the net power absorbed from the public network (15), combined with the full expression for the building consumption as expressed in (7):

$$P^g(k) = \sum_{i=1}^{N^{st}} P_i^{st}(k) + \sum_{b=1}^{N^{bu}} P_b^{bu}(k) + P^{PV}(k) = \\ = \sum_{i=1}^{N^{st}} P_i^{st}(k) + \sum_{b=\{A,B\}} \left(P_b^{el}(k) + \sum_{n=1}^{N_b^{tz}} \frac{\dot{Q}_{n\,b}(k)}{COP_{n\,b}} \right) + P^{PV} \quad (15)$$

Following the procedure introduced in Section 2.1, a binary variable $\delta^g(k) \in \{0,1\}$ defined by (15) takes into account the sign associated with the power flow at the point of coupling with the external public network; as a convention, $P^g(k) \geq 0$ when the physical electrical power flows from the public network to the microgrid:

$$P^g(k) \geq 0 \;\leftrightarrow\; \delta^g(k) = 1 \quad (16)$$

The binary variable $\delta^g(k)$ defined by (16) can be expressed through the mixed-integer linear inequality system (17), following the same procedure already introduced in (3) for the battery storage devices:

$$\begin{cases} P^g(k) - \left(\overline{P^g} + \varepsilon\right)\delta^g(k) + \varepsilon \leq 0 \\ -P^g(k) + \underline{P^g}\left(1 - \delta^g(k)\right) \leq 0, \end{cases} \quad (17)$$

with $P^g(k) \in \left[\underline{P^g}; \overline{P^g}\right]$.

The introduction of the binary variable δ_g allows to correctly track the sign of the power flow with the external public network and hence take into account the difference between the buy and sell energy prices typically applied by Distribution System Operators and the environmental impact associated to the microgrid operational profile, as clarified in Section 3.1.

2. System optimization

The system-level MPC scheme is described in this section. At each time step an optimization problem is solved and the first input of the obtained optimal trajectory is applied to the system. The procedure is repeated at each point in time, updating the states with the latest measurements and forecasts available, thus potentially compensating for any unpredicted disturbance in the models. Two counterposed objectives are included in the cost function of the MPC problem:

a) energy arbitrage and minimization of the system operating cost associated with the battery ageing: these costs are expressed as a monetary net gain or loss for the system;
b) minimization of the carbon impact of the exchanged energy profile with the network.

2.1. Energy price arbitrage

Consider the typical time-varying profiles (as the ones shown in Fig. 3) which represent the evolution of the buy/sell prices (λ_b and λ_s respectively) associated to the energy exchanged with the external public network. Exploiting the δ^g definition proposed in (16), buy λ_b / sell λ_s price difference can be expressed as:

$$C_A = \Delta t \sum_{k=1}^{H} \left\{ \left[\lambda_b(k)\delta^g(k) + \lambda_s(k)\left(1 - \delta^g(k)\right) \right] P^g(k) \right\}. \quad (18)$$

The bilinear relation term in equation (18) $\delta^g \cdot P^g$ can be rewritten in a MILP form through the introduction of an additional variable $z^g(k) = P^g(k) \cdot \delta^g(k)$ and the set of liner inequalities (19), as the ones introduced for the storage devices in (5). The reformulated linear cost function is reported in (20).

$$\begin{cases} z^g(k) - \overline{P^g}\,\delta^g(k) \leq 0 \\ -z^g(k) + \underline{P^g}\,\delta^g(k) \leq 0 \\ z^g(k) - P^g(k) + \underline{P^g}\left(1 - \delta^g(k)\right) \leq 0 \\ -z^g(k) + P^g(k) - \overline{P^g}\left(1 - \delta^g(k)\right) \leq 0 \end{cases} \quad (19)$$

$$C_A = \Delta t \sum_{k=1}^{H} \left\{ \lambda_b(k) z^g(k) + \lambda_s(k) P^g(k) - \lambda_s(k) z^g(k) \right\}. \quad (20)$$

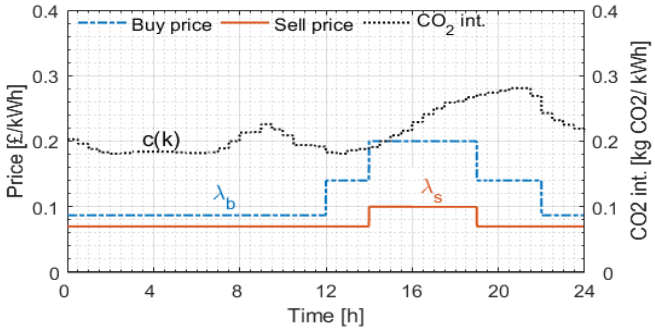

Fig. 3: Buy λ_b and sell λ_s prices (assumed as known) for the considered case study, together with the day-ahead forecasted Carbon Intensity $c(k)$ for UK [25].

2.2. Carbon intensity reduction

Increasing public concerns about the environmental impact and sustainability of daily activities is reflected by the adoption of minimally impacting energy behaviours. The environmentally concerned user can also consciously decide to minimize their carbon footprint. Therefore a carbon related cost C_{CI} term (18) is included in the problem formulation, which considers the forecast Carbon Intensity $c(k)$ of the energy consumption (Fig. 3, secondary axis) [24], weighted by a user-defined sustainability factor λ_{CI} in $£/gCO_2$, which represents the acceptable net-loss incurred by the user to avoid the emission of a gCO_2 associated with their consumption profile.

$$C_{CI}=\lambda_{CI}\Delta t\sum_{k=1}^{H}c(k)\delta^{g}(k)P^{g}(k)= \\ =\lambda_{CI}\Delta t\sum_{k=1}^{H}c(k)z^{g}(k). \tag{21}$$

The weighting coefficient $\lambda_{CI}\in[0;+\infty)$ in (21) represents the users disposition to adopting a carbon-free energy pattern rather than just maximizing economic profit, leading to a Pareto curve, rather than to a single optimized profile. For $\lambda_{CI}=0$, the economic profit is maximized independent of the carbon footprint, while for increasing values of $\boldsymbol{\lambda_{CI}}$ a more environmentally sustainable energy plan is preferred. Carbon Intensity predictions $c(k)$ are available for UK in [25].

2.3. Battery ageing model

A battery ageing model is included in the optimization problem to account for the capital amortization due to the effect of the optimized control on the storage capacity. Wear-out phenomena are modelled in the cost function as additional terms, which take into account the battery power usage pattern [26]. Two different effects need to be taken into account:

- wear-out which is directly proportional to the amount of cycled energy. This effect can be modelled as in (22), where λ_{1i} is the cost per cycle of the i-th unit.

$$C_1=\sum_{i=1}^{N^{st}}\left(\frac{\lambda_{1i}\Delta t}{2\,E_i}\sum_{k=1}^{H}|P_i^{st}(k)|\right) \tag{22}$$

- given the same exchanged energy, higher power levels induce faster battery ageing, thus a term, (23), proportional to the maximum absolute power is needed.

$$C_2=\sum_{i=1}^{N^{st}}\left(\lambda_{2i}\max_{k\in[1;H]}|P_i^{st}(k)|\right) \tag{23}$$

The absolute value function in (22)-(23) can be easily expressed in a MILP form through a standard procedure similar to the one already introduced for the non-linear storage behaviour in (2).

2.4. MPC problem formulation

The MPC algorithm is set as a minimization problem over the prediction horizon H. The objective function is defined as $J(u,f)=C_A(u,f)+C_1(u,f)+C_2(u,f)+C_{CI}(u,f)$, where u is the vector of decision variables and f of the forecasts:

$$u=\{P_i^{st}\ SoC_i\ \delta_i^{st}\ z_i^{st}\ \dot{Q}_{nb}\ \vartheta_{nb}\ P^{g}\ \delta^{g}\ z^{g}\},$$
$$f=\{P_b^{el}\ \ Irr^{h}\ \ P^{PV\,h}\},\ n\in 1\dots N_b^{tz},\ b=\{A,B\}.$$

The physical parameters of the storage devices and buildings, as well as the time profiles of the buy $\lambda_b(k)$ and sell $\lambda_s(k)$ prices and carbon intensity $c(k)$ are assumed known. The sustainability factor λ_{CI} involved in the definition of C_{CI} is a user-defined parameter.

Thus the MPC problem can be formulated as follows:

$$\min_{u} J(u,f)$$

subject to the following constraints:

Storage asset

- Equality constraint (4)
- Inequality constraint (6)

Buildings

- Equality constraint (8)
- Thermal comfort $\vartheta_{n\,b}(k)\in\left[\underline{\vartheta_{n\,b}};\ \overline{\vartheta_{n\,b}}\right]$, for $b=\{A,B\},\ n=1..N_b^{tz}$

Grid balance

- Equality constraint (15)
- Inequality constraints (17)-(19).

3. Experimental set-up description

The validation of the proposed MPC framework has been carried out considering a microgrid which uses sustainable power technologies. The microgrid consists of an energy storage asset, which has flexibility in its control, a PV system and two smart-buildings, which enable flexibility due to each having three thermal zones. The full experimental setup is shown in Fig. 4, where hardware and simulated elements are combined together to test the actual algorithm capabilities on physical grid-scale devices.

3.1. Power Hardware and HIL

The power hardware is a 240 kVA 180 kWh commercial lithium-ion battery storage device from Siemens, which is equipped with a local controller, and is interfaced to external systems by a dSpace DS1007 control box. As depicted in Fig.4, the dSpace unit implements the battery storage control through a typical grid-following scheme [27], actuating the power set-point commands received from the real-time digital simulator (RTDS Technologies) and sending, as a feedback, the measured phase currents at the converter terminals.

The RTDS unit purpose is twofold. On one side, it simulates all the microgrid assets other than the power hardware during the real-time operations, i.e. electro / thermal behaviour of the buildings, external variable frequency network and PV power plant, with a discretization step $T_s=100\mu s$. Thus the RTDS represents the central processing unit were all the physical/simulated quantities are managed and dispatched. On the other hand, it operates as a communication gateway with the MATLAB environment, where the MPC optimal problem is implemented and solved: the state variables of the system during the real-time operations are sent from the RTDS to MATLAB,

which are used as the inputs of the optimization problem. The power set-points calculated by the MATLAB environment are sent back to each asset to be tracked.

The design characteristics for the set-up are reported in Tables I and II (a more detailed characterization of the energy storage asset is available in [28]), while the numerical values needed for the battery ageing model (Section 3.2) are derived from [29] and are listed in Table III.

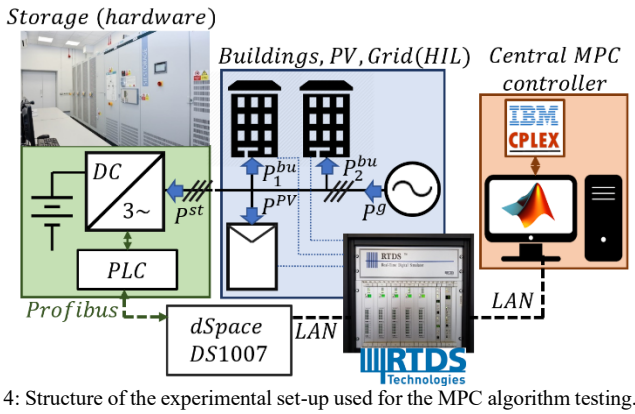

Fig. 4: Structure of the experimental set-up used for the MPC algorithm testing.

TABLE I: ENERGY STORAGE AND PV SYSTEM PARAMETERS

Coefficient	*Value*	*Unit*
$\underline{P^{st}}, \overline{P^{st}}$	-200, 200	kW
$\underline{SoC}, \overline{SoC}$	10%, 90%	%
E	180	kWh
η_{ch}, η_{dis}	92%	%
$\overline{P^{PV}}$	240	kW
ϕ	43° North	deg.
$\Delta t, H$	15, 48	min, -

TABLE II: BUILDING PARAMETERS

Build.	*Coefficient*	*Value*	*Unit*
A	$C_{1A}^{th}, C_{2A}^{th}\ C_{3A}^{th}$	0.88, 0.21, 0.18	MJ/K
	$G_{1A}^{th}, G_{2A}^{th}, G_{3A}^{th}$	18.2, 2.60, 3.57	W/K
	p_{1A}, p_{2A}, p_{3A}	15.2, 4.84, 3.01	W
	s_{1A}, s_{2A}, s_{3A}	22.0, 8.38, 6.28	m²
B	$C_{1B}^{th}, C_{2B}^{th}, C_{3B}^{th}$	1.0, 1.2, 0.49	MJ/K
	$G_{1B}^{th}, G_{2B}^{th}, G_{3B}^{th}$	14.3, 98.2, 28.6	W/K
	p_{1B}, p_{2B}, p_{3B}	0.68, 0.51, 0.29	W
	s_{1B}, s_{2B}, s_{3B}	0.79, 2.12, 1.04	m²
A/B	k_p, k_i	2, 4e-3	kW/K, kW/(Ks)
	$[\underline{\vartheta_n}; \overline{\vartheta_n}], COP$	[19;22], 1.5	[°C; °C], W/W

TABLE III: COST PARAMETERS

Coefficient	*Value*	*Unit*
λ_1	7.5e-03	£/kWh
λ_2	6.75e-04	£/kW
$\lambda_b(t), \lambda_s(t)$	see Fig. 3	£/kWh
$c(k)$	see Fig. 4	gCO_2/kWh
λ_{CI}	[0 0.001 0.005 0.01]	£/gCO_2

3.2. *Computational aspects*

The solution of the MPC algorithm in MILP form is obtained in the MATLAB environment by using the IBM-CPLEX solver, suitably implemented by using he MATLAB-based optimization tool YALMIP [30]. The MPC problem is performed considering a sampling period Δt equal to 15 minutes and a half-day total prediction horizon (H = 48). Since binary variables are employed to represent the battery storage dynamics (see eq. (6)), the MPC optimization model is cast as a Mixed Integer Linear Program (MILP), which can be efficiently solved through the CPLEX Branch-and-Bounds algorithm. On a 64-bits architecture based on the Intel® Core™ i7-6700 CPU 3.40 GHz processor, equipped with a 16.0 GB RAM memory, the computational time associated to the solution of the MPC problem at each time step is bounded within 10s – 25s, with an average value close to 15s. Being the computation time significantly lower than the sampling period Δt, a higher number of controlled devices could be easily included and managed. The MATLAB is interfaced with the RTDS system through the freeware JTCP library, which enables a TCP-based communication from MATLAB to the real-time simulator.

3.3. *Scenario Descriptions*

Three different scenarios are considered to test the proposed optimization scheme under increasing levels of flexibility from sustainable energy assets.

CS0, Scenario 0 (base case): the system is operated without any flexibility from assets. The storage unit is neglected. The temperature control within the buildings is carried out by simple local proportional-integral (PI) controllers, which are responsible for the thermal management within each thermal zone, in terms of their heat injection ($\dot{Q}_n$, for $n \in 1 \dots N_b^{tz}$, $b \in 1 \dots N^{bu}$). This serves as a base case benchmark to assess the performances of the MPC algorithm.

CS1, Scenario 1 (electrical flexibility): the system is operated assuming that the MPC exclusively manages the energy storage asset. The buildings thermal control is the same as in *CS0*.

CS2, Scenario 2 (electrical and thermal flexibility): the system is operated exclusively by the MPC scheme described in Section 3, which is able to integrate the thermal and electrical dynamics within a unique optimization framework.

In scenarios *CS0* and *CS1*, a PI controller with a constant reference equal to the mean value of the comfort range is adopted to manage the heat injections $\dot{Q}_n(k)$ for each thermal zone to maintain the temperature $\vartheta_n(k)$ within the comfort range $[\underline{\vartheta_n}; \overline{\vartheta_n}]$. In scenario 2, *CS2*, the thermal behaviour is controlled by the MPC algorithm.

4. Experimental results

4.1. *Carbon impact and energy cost reduction (CS1)*

Scenario 1 CS1 (electrical flexibility) has been experimentally tested using the actual building load and weather data from Monday the 2nd of April 2018; for this day, the load forecaster has a RMSE of 7.4 kW (building 1) and 12.3 kW (building 2), while the hybrid PV forecaster RMSE is 56.2 W/m².

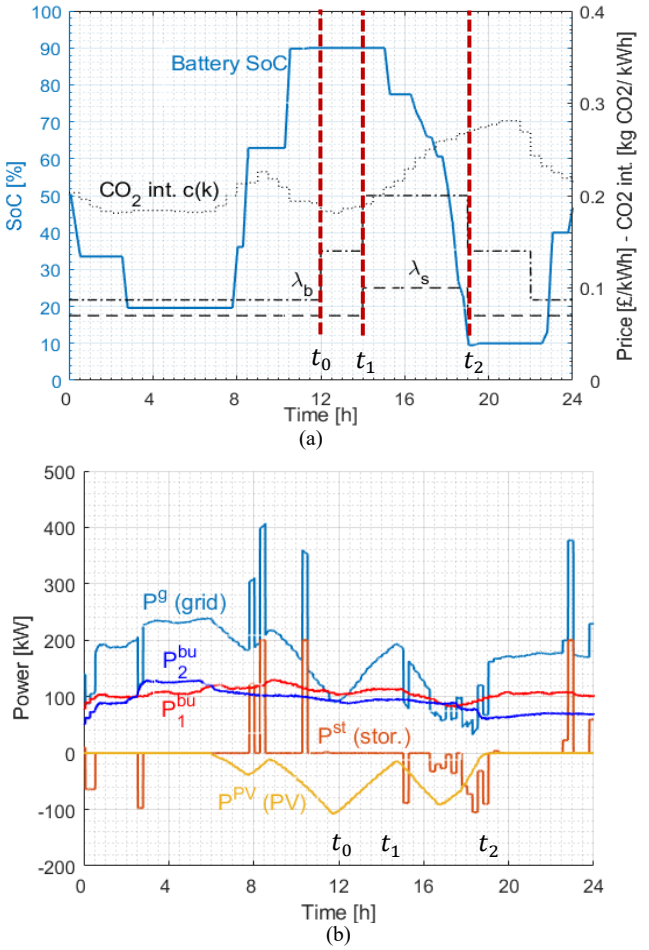

Fig. 5: *Scenario 1 CS1* - SoC, buy/sell prices, equivalent carbon intensity (a) and power profiles (b), λ_{CI}=0. As a convention, all the powers are positive when absorbed from the network.

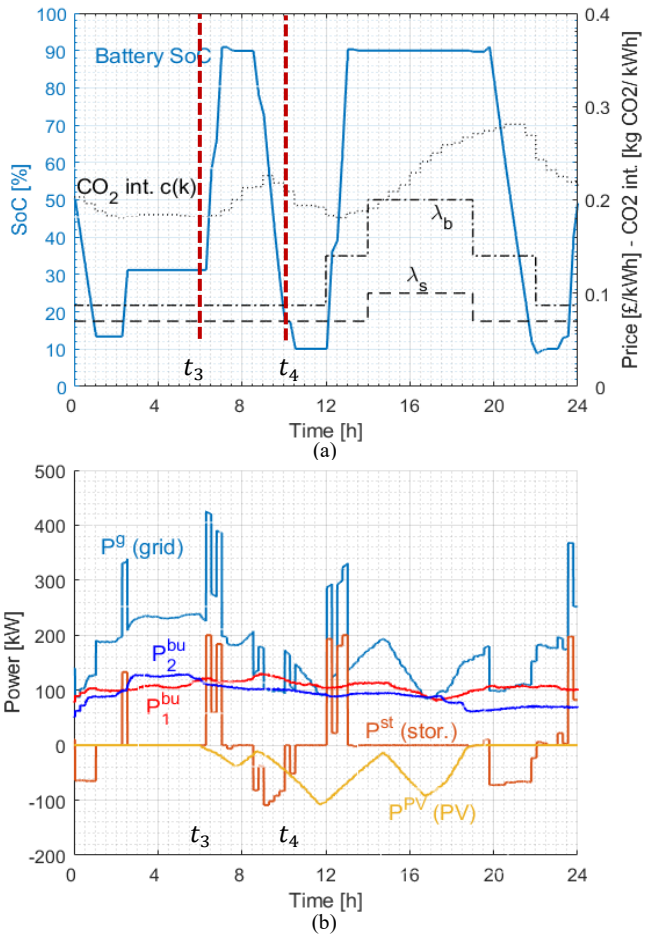

Fig. 6: *Scenario 1 CS1*- SoC, buy/sell prices, equivalent carbon intensity (a) and power profiles (b), with λ_{CI}=0.05. As a convention, all the powers are positive when absorbed from the network.

Fig. 5 shows the experimental test data for $\boldsymbol{\lambda_{CI}}$ =0 which means the optimization only considers economic factors: Fig. 5(a) shows the profile of the battery state of charge, where the MPC utilizes the change in energy buy price $\boldsymbol{\lambda_b}$ (occurring between t_0=12 noon and t_1=2 p.m.) by pre-emptively charging the storage asset and subsequently discharging the battery as the energy sell price $\boldsymbol{\lambda_s}$ was at a maximum (between t_1=2 p.m. and t_2 =7 p.m.). The corresponding power profiles for all assets are shown in Fig. 5(b), where the discharge operation of the storage asset during the high sell price conditions time period (t_1 to t_2) is visible. For the same day of data, the *base case* (*CS0*, no flexibility) has an equivalent energy consumption of 478 £/day and 875 kgCO_2/day, whereas *CS1* has an equivalent energy consumption of 462 £/day and the same CO_2 profile (as $\boldsymbol{\lambda_{CI}}$=0).

The sustainable technology weighting factor $\boldsymbol{\lambda_{CI}}$ is increased to $\boldsymbol{\lambda_{CI}}$=0.05 $£/gCO_2$ in Fig. 6. The MPC balances the economic profit with the minimization of the environmental impact of the absorption pattern. Hence, an additional charge/discharge cycle (Fig. 6(a), between t_3= 6 a.m. and t_4= 10 a.m.) occurs to reduce the consumption from the external grid in response to the forecasted peak in carbon intensity, at approximately t_4. When comparing Fig. 5 and Fig. 6, the non-zero λ_{CI} also causes the MPC to modify the operation of the storage asset in response to the high sell price (t_1 to t_2) as this time period is immediately before a time period of high CO_2 intensity. In Fig. 6 the MPC charges the storage asset when the energy buy price is low, and then discharges the storage asset when the CO_2 intensity is high. The energy consumption in this case is minimally affected by the control but the CO_2 impact reduces to 863 kgCO_2/day.

4.2. Building thermal dynamics contribution (CS2)

By including the building thermal dynamics in the optimization problem (case *CS2)* both electrical and thermal flexibility in the sustainable assets can be co-optimized, increasing the algorithm performances. Fig. 7 shows the experimental results for the same day as used in Figs. 5 and 6. Temperature profiles for all three thermal zones in Building 1 are shown in Fig. 7, with Fig. 7(a) being for *CS1*, and Figure 7(b) referred to the case *CS2*.

The PI-based regulation in *CS1* shows poor rejection of the external solar radiation P^{PV} and occupancy (Fig. 7(a)), leading to unregulated oscillations of the temperatures profiles (for clarity, its equivalent regulation scheme is reported in Fig.8). The PI-based regulation scheme requires to set an average reference temperature within the comfort range and to compensate the unpredicted positive and negative variations caused by the solar radiation and building occupancy.

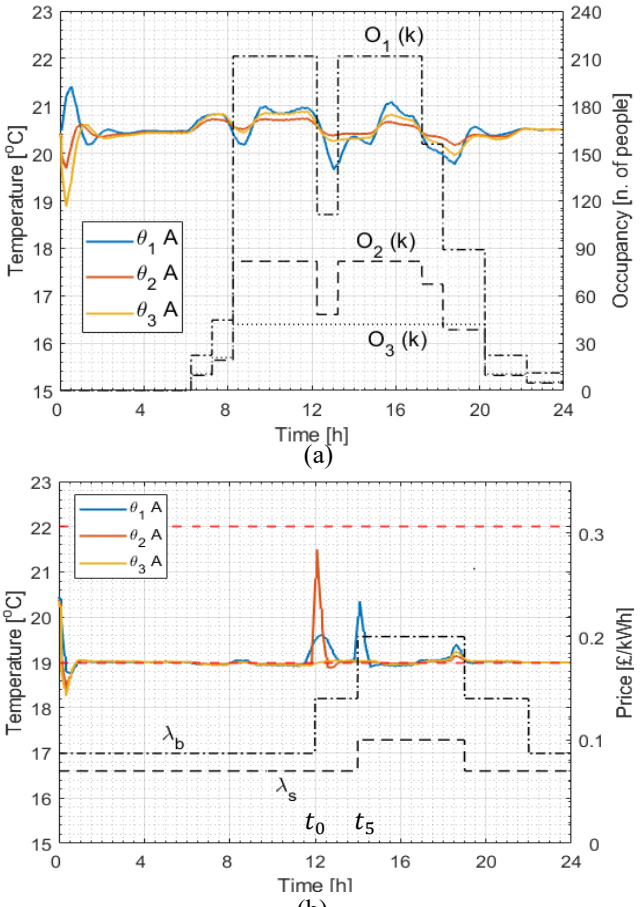

Fig. 7: Thermal zone temperatures (ϑ_1,ϑ_2,ϑ_3) for building 1 under (a) *CS1* (*CS1*: electrical flexibility) or (b) *CS2* (*CS2*: electrical + thermal flexibility).

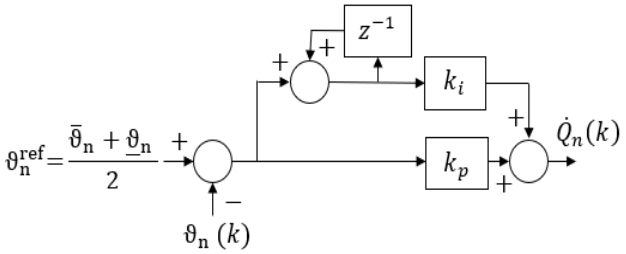

Fig. 8: Equivalent scheme of the discretized PI controller as exploited in *CS1*.

The possibility to include the compensation of the external disturbances (e.g. building occupancy and irradiance) directly into the MPC optimization problem (Fig. 7(b)) represents a key advantage of the proposed architecture over the simpler un-compensated scheme reported in Fig. 8. The MPC approach reduces the occurrence and frequency of the thermal zones' temperature oscillations, thus increasing the comfort for the building occupiers. Its predictive capabilities enable the retention of a slightly lower average temperature inside each thermal zones without violating the comfort constraint $\vartheta_n(k) \in \left[\underline{\vartheta_n}; \overline{\vartheta_n}\right] = [19; 22]$ °C. This leads to a reduced energy consumption and carbon impact in *CS2* with respect to the scenario *CS1*. Additionally, the MPC optimally manages the amount of stored heat inside the building so as to minimize the energy consumption of the premises: as soon as a step-increase of the buy price is foreseen (e.g. at t_0=12 noon), the control system stores thermal energy within the building, which later allows a natural temperature decrease during the first time steps after the price rise, in order to reduce the corresponding cash flow associated to the energy absorption. This phenomenon can be observed from the temperature peaks experienced at t_0=12 noon and t_5= 2 p.m. in Fig. 7(b); the thermal comfort constraints are not violated thanks to the inclusion of the characteristic dynamics of each zone within the model. It is worth highlighting how this behaviour is mainly due to the energy-arbitrage revenue maximization included in the cost function definition; if this is not desired, it could be easily removed through a different formulation of the MPC cost terms.

The predictive nature of MPC allows taking advantage of the flexibility in the temperature comfort range and optimizing the stored heat inside the building. This leads to an improvement of the system energy behaviour demonstrated by an energy saving of almost 50£/day for *CS2* with respect to *CS0* (compared to 16£/day for *CS1*), where a PI is utilized.

Without loss of generality and for the sake of simplicity, the sustainable technology weighting coefficient $\boldsymbol{\lambda_{CI}}$ was set to 0 for both cases reported in with Fig. 7(a) and with Fig. 7(b), implying an optimization focused on the economic profit only.

4.3. *Results evaluation*

A more comprehensive evaluation of the MPC algorithm performance is given in Fig. 9, which shows the energy savings and CO_2 emission reduction for different values of the sustainable technology carbon weighting factor $\boldsymbol{\lambda_{CI}}$. The combination of the optimal solutions corresponding to different values of the weighting factor λ_{CI} defines a Pareto curve in the space of the solutions. The coordinated management of the electrical/thermal dynamics (*CS2*) increases the degree of flexibility associated with the optimization problem and guarantees better performance both in terms of carbon reduction and energy cost containment.

Referring to the results associated with *Scenario 2 CS2*, the proposed MPC-based optimal management guarantees a CO_2 reduction of up to 75 kg/day ($\boldsymbol{\lambda_{CI}}$=0.01 £/g$CO_2$) and a maximum energy saving of up to 50 £/day ($\boldsymbol{\lambda_{CI}}$ =0) with respect to the base case *CS0*. *CS2* also yielded a 350% energy saving when compared to *CS1* ($\boldsymbol{\lambda_{CI}}$=0), and a 400% CO_2 saving when compared to the savings in *CS1*, showing the significant performance improvement if all available flexibility is utilized.

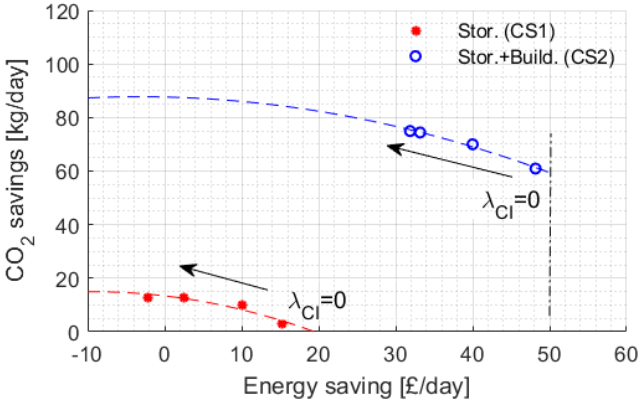

Fig. 9: Energy and CO_2-emission savings, for different values of sustainability technology factor λ_{CI}, for the two considered case studies (*CS1*: electrical flexibility, *CS2*: electrical and thermal flexibility).

5. Conclusion

A detailed system-level optimization method has been described for use with sustainable technology systems which have flexibility in their operating characteristics. The optimization has been demonstrated using a microgrid rich in sustainable energy systems. Key innovative aspects have been included in the optimization framework, such as non-ideal conversion efficiencies for battery storage, flexibility in electrical/thermal loads and detailed battery degradation models. The proposed MPC problem is multi-objective, and its parameters can be set so as to maximize the profit from energy arbitrage, to minimise carbon emissions, or to optimize both criteria simultaneously: this feature represents a key element in the light of the rising concerns about the environmental sustainability of the current energy production, distribution and consumption paradigms. A hybrid estimator of the PV production based on clear-sky models and actual irradiance measurements is proposed, suitable for real-time operation.

A further novelty of the proposed MPC approach regards its experimental testing. The MPC algorithm has been demonstrated experimentally using a HIL system together with an actual grid-scale battery energy storage system connected to the UK public power network. Three scenarios were demonstrated with different levels of flexibility in the electrical and thermal loads. When the both electrical and thermal loads flexibility was utilised by the MPC (*CS2*), a CO_2 reduction of up to 75 kg/day ($\boldsymbol{\lambda_{CI}}$=0.01 £/gCO2) and a maximum energy saving of up to 50 £/day ($\boldsymbol{\lambda_{CI}}$=0) with respect to the base case *CS0* was achieved. When electrical and thermal flexibility (*CS2*) is compared to electrical only flexibility (*CS1*) then a 350% energy saving (and $\boldsymbol{\lambda_{CI}}$=0), and a 400% CO_2 saving were achieved.

References

[1] United Nations Environment Program, “Global Environment Outlook – GEO-6: Healthy Planet and People,” Cambridge Uni. Press, May 2019.

[2] National Grid, “The future of Gas - How gas can support a low carbon future,” and “Future Energy Scenarios” 2018

[3] J. A. Rossiter, *Model-based predictive control: A practical approach*. Sheffield, CRC Press, pp. 1-318, 2017.

[4] A. La Bella, S. Raimondi Cominesi, C. Sandroni, and R. Scattolini, “Hierarchical Predictive Control of Microgrids in Islanded Operation,” *IEEE Trans. Autom. Sci. Eng.*, vol. 14, no. 2, pp. 536–546, Apr. 2017.

[5] T. Morstyn, B. Hredzak, R. P. Aguilera, and V. G. Agelidis, “Model Predictive Control for Distributed Microgrid Battery Energy Storage Systems,” *IEEE Trans. Control Syst. Technol.*, vol. 26, no. 3, pp. 1107–1114, May 2018.

[6] A. Parisio, E. Rikos, and L. Glielmo, “A Model Predictive Control Approach to Microgrid Operation Optimization,” *IEEE Trans. Control Syst. Technol.*, vol. 22, no. 5, pp. 1813–1827, Sep. 2014.

[7] D. Zhao, H. Wang, J. Huang, and X. Lin, “Virtual Energy Storage Sharing and Capacity Allocation,” *IEEE Trans. Smart Grid*, vol. 11, no. 2, pp. 1112–1123, 2020.

[8] X. Zhu, J. Yang, Y. Liu, C. Liu, B. Miao, L. Chen, “Optimal scheduling method for a regional integrated energy system considering joint virtual energy storage,” *IEEE Access*, vol. 7, pp. 138260–138272, 2019.

[9] F. Oldewurtel *et al.*, “Use of model predictive control and weather forecasts for energy efficient building climate control,” *Energy Build.*, vol. 45, pp. 15–27, Feb. 2012.

[10] D. Sturzenegger, D. Gyalistras, M. Morari, and R. S. Smith, “Model Predictive Climate Control of a Swiss Office Building: Implementation, Results, and Cost-Benefit Analysis,” *IEEE Trans. Control Syst. Technol.*, vol. 24, no. 1, pp. 1–12, 2016.

[11] J. Leithon, S. Sun, and T. J. Lim, "Demand Response and Renewable Energy Management Using Continuous-Time Optimization," *IEEE Trans. on Sustainable Energy*, vol. 9, no. 2, pp. 991-1000, April 2018.

[12] H. Hao, D. Wu, J. Lian and T. Yang, "Optimal Coordination of Building Loads and Energy Storage for Power Grid and End User Services,"*IEEE Trans. on Smart Grid*, vol. 9, no. 5, pp. 4335-4345, Sept. 2018.

[13] Y. Zhang and Q. Jia, "A Simulation-Based Policy Improvement Method for Joint-Operation of Building Microgrids With Distributed Solar Power and Battery," *IEEE Trans. on Smart Grid*, vol. 9, no. 6, pp. 6242-6252, Nov. 2018.

[14] J. Niu, Z. Tian, Y. Lu and H. Zhao, "Flexible dispatch of a building energy system using building thermal storage and battery energy storage," *Applied Energy*, vol. 243, pp.274-287, June 2019.

[15] E. Biyik, A. Kahraman, “A predictive control strategy for optimal management of peak load, thermal comfort, energy storage and renewables in multi-zone buildings”, *Journal of Building Engineering*, n. 25, art. no. 100826, Sept. 2019.

[16] H. P. Williams, *Model Building in Mathematical Programming*, 5th ed. Wiley and Sons, 2013.

[17] A. Parisio, M. Molinari, D. Varagnolo, and K. H. Johansson, “Energy Management Systems for Intelligent Buildings in Smart Grids,” in *Advances in Industrial Control*, no. 9783319684611, 2018, pp. 253–291.

[18] A. Parisio and S. P. Gutierrez, “Distributed model predictive control for building demand-side management,” in *2018 European Control Conference (ECC)*, 2018, pp. 2549–2554.

[19] P.N. Paraskevopoulos, *Modern Control engineering,* CRC Press, Athens, pp. 1-736, 2017.

[20] G. W. Chang and H. J. Lu, “Integrating Grey Data Preprocessor and Deep Belief Network for Day-ahead PV Power Output Forecast,” *IEEE Trans. Sustain. Energy*, vol. 3029, no. c, 2018.

[21] E. Ogliari, A. Bolzoni, S. Leva, and M. Mussetta, “Day-ahead PV Power Forecast by Hybrid ANN Compared to the Five Parameters Model Estimated by Particle Filter Algorithm,” in *Lecture Notes in Computer Science*, vol. 9887 LNCS, 2016, pp. 291–298.

[22] A. Nespoli et al., “Day-ahead photovoltaic forecasting: A comparison of the most effective techniques,” *Energies*, vol. 12, no. 9, pp. 1–15, 2019.

[23] F. Antonanzas-Torres, R. Urraca, J. Polo, O. Perpiñán-Lamigueiro, and R. Escobar, “Clear sky solar irradiance models: A review of seventy models,” *Renew. Sustain. Energy Rev.*, vol. 107, no. March 2018, pp. 374–387, 2019.

[24] K. Paridari, A. Parisio, H. Sandberg, and K. H. Johansson, “Robust Scheduling of Smart Appliances in Active Apartments With User Behavior Uncertainty,” *IEEE Trans. Autom. Sci. Eng.*, vol. 13, no. 1, pp. 247–259, Jan. 2016.

[25] National Grid ESO, “Carbon Intensity API.” [Online]: https://carbonintensity.org.uk/.

[26] J. M. Reniers, G. Mulder, S. Ober-Blöbaum, and D. A. Howey, “Improving optimal control of grid-connected lithium-ion batteries through more accurate battery and degradation modelling,” *J. Power Sources*, vol. 379, pp. 91–102, Mar. 2018.

[27] A. Bolzoni and R. Perini, "Feedback Couplings Evaluation on Synthetic Inertia Provision for Grid Frequency Support," in *IEEE Trans. on Energy Conversion*, 2020, Early access. DOI: 10.1109/TEC.2020.3021305.

[28] A. Bolzoni, Q. Zhu, V. Tsormpatzoudis, R. Todd, and A. Forsyth, “Dynamical Characterization of Grid-Scale Energy Storage Assets,” in 45th *Industrial Electronics Annual Conference (IECON)*, Lisbon, 2019.

[29] S. Liu, A. Forsyth and R. Todd, "Battery Loss Modelling Using Equivalent Circuits," *2019 IEEE Energy Conversion Congress and Exposition (ECCE)*, Baltimore, MD, USA, 2019, pp. 2478-2484.

[30] J. Löfberg, YALMIP toolbox for modeling and optimization in MATLAB, [Online]: https://yalmip.github.io/